machines

MDPI

Article

Lumped Parameter Model for Structural Analysis of Over-Constrained Multi-Legged Parallel Mechanism Supporting System Applied to Cryogenic Devices

Luca Piacentini [1,*], Luca Dassa [2], Diego Perini [2], Andris Ratkus [1], Toms Torims [1] and Stefano Uberti [3]

[1] Institute of Particle Physics and Accelerator Technologies, 1048 Riga, Latvia
[2] Organisation Européenne pour la Recherche Nucléaire, 1211 Geneve, Switzerland
[3] Department of Mechanical and Industrial Engineering, University of Brescia, 25123 Brescia, Italy
* Correspondence: luca.piacentini@rtu.lv

Abstract: While the design of a cryostat is being developed, one of the most relevant sub-systems is the internal supporting system that sustains the cooled component. According to the literature, the arrangement and number of supports chosen often result in a multi-leg over-constrained architecture. These are usually studied by means of finite element analysis tools alone, which makes studies like the optimization of supporting systems computationally expensive. This paper proposes a more structured and general analytical model compared to the existing models for this application. The proposed lumped parameter model allows designers to study the influence of external loads, pre-load, and cool-down on stress levels and deformation status of the supports of the cryogenic device as well as the consequent misalignment of the cooled component. The general lumped parameter model for n tie-rods of different shapes, dimensions, and materials is proposed. Two particularized models of eight and eleven supports are validated by comparing the results with those from standard finite element analysis software. Results show that the proposed model has a strong agreement with finite element simulations, and the median of relative errors is about 1.4%. This accuracy is obtained for models of randomly arranged supports, which proves the effectiveness of the model in predicting results even for non-symmetrical support configurations. Comparable and accurate results are obtained, which are about 130 times faster than in finite element analysis, thus proving the effective reduction in computational cost. Additionally, the proposed code lets designers change input parameters in a quicker and reliable way.

Keywords: cryostat; supporting system; analytical model; over-constrained

check for updates

Received: 12 December 2024
Revised: 5 February 2025
Accepted: 6 February 2025
Published: 8 February 2025

Citation: Piacentini, L.; Dassa, L.; Perini, D.; Ratkus, A.; Torims, T.; Uberti, S. Lumped Parameter Model for Structural Analysis of Over-Constrained Multi-Legged Parallel Mechanism Supporting System Applied to Cryogenic Devices. *Machines* **2025**, *13*, 129. https://doi.org/10.3390/machines13020129

Copyright: © 2025 by the authors. Licensee MDPI, Basel, Switzerland. This article is an open access article distributed under the terms and conditions of the Creative Commons Attribution (CC BY) license (https://creativecommons.org/licenses/by/4.0/).

1. Introduction

One of the most important sub-systems of a cryostat in a cryogenic device [1,2] is its supporting system. This system must be able to sustain heavy masses while limiting the heat flux to a cooled component. The arrangement, number, dimensions, and material of the supporting elements must be defined during the design of the supporting system. The optimization of the arrangement of supports allows us to meet accuracy/mechanical resistance requirements and minimize heat flux to the cold mass. For instance, changing the arrangement of supports allows us to reduce support internal actions due to external loads, differential thermal contraction, pre-load, etc. The reduction of internal actions allows the designer to size smaller support transversal sections (having fixed a minimum

safety factor), effectively minimizing heat flux and, thus, operational costs for the cryogenic cooling system.

With regard to supporting systems of cryogenic devices found in the literature [3], which are mostly based on an over-constrained tie-rod architecture and have been used for superconducting magnets in the physics research field [4–9] as well as for the Medical applications [10], a mathematical model has been proposed to evaluate only the internal loads in the particular case of an eight symmetric supporting system [11]. Over-constrained systems, unlike exactly constrained ones, require additional equations with respect to classic equilibrium equations in order to calculate reaction forces and displacements of points in the system. As highlighted from the previous literature review [3], all of the systems appear to have been studied only by finite element analysis (FEA) [12] approaches to evaluate the loads and displacements necessary for design choices such as materials and dimensions of the supports. Only one mathematical model has been proposed to evaluate the internal actions on supports of an eight symmetric supporting system in a cryostat [11]. A comprehensive review of the over-constrained parallel mechanisms [13], which were used for different applications, describes different methods to solve the statically indeterminate system associated to a parallel mechanism under external loads. However, the contribution of a thermal gradient on the supports is not considered. This is of paramount importance for the application of passive parallel mechanisms studied in this article.

This work proposes a generic semi-analytical model of the supporting system of a cryogenic device supported by any number of tie rods ($n \geq 6$). It improves from the previous models, which are limited by the symmetry of the architecture and the number of rods being considered, and fills the knowledge gap with a more structured study and general model. This model takes the dimensions, material, and the generic arrangement of the tie rods as input. The model enables us to calculate the internal loads for all supports and the displacement (all six DOF) of the cryogenic device as an effect of a generic external load $(F_x, F_y, F_z, M_x, M_y, M_z)$, pre-load on each support, and vacuum and thermal contraction due to cool-down. These results are usually achieved, thanks to FEA. Optimization and sensitivity analysis of such systems using a classic FEA is computationally expensive. The model proposed in this work produces, in a computationally cheaper way, results that are in strong agreement with those calculated by a popular and acknowledged software for FEA. This model opens the possibility for designers to run extensive optimization routines and comprehensive sensitivity analysis, helping us to better grasp the interplay of input parameters and desired outputs.

The outline of the paper is as follows:

- The generic analytical model for any number of tie-rods is formulated in Section 2;
- The setup of validation simulations in two study cases of eight and eleven supports is reported in Section 3;
- The results of the validation are discussed in Section 4;
- A particularized version of general equations is reported in detail in Appendix A;
- An example of the implementation of the code in Wolfram Mathematica [14] is given in Appendix B;
- An example of the possible application of the code to a real study case is given in Appendix C.

2. Lumped Parameter Model

Structurally, the essential components of a cryostat for a cryogenic device are the supports and the vacuum vessel (Figure 1). The model for the estimation of all displacements and rotations of the cryogenic device in the space will be referred to as the Lumped Parameter error Model or simply LPM. For over-constrained supporting systems of cryogenic

devices, the calculation of loads and displacements must take into account the contributions of both the vacuum vessel stiffness and the stiffness of supports. Classical loading conditions require us to study the application of generic external loads, pre-load on the supports, and internal stress due to cool-down and vacuum pressure inside the vessel. The formulation of a model that implements the contributions listed above is given in the following paragraphs.

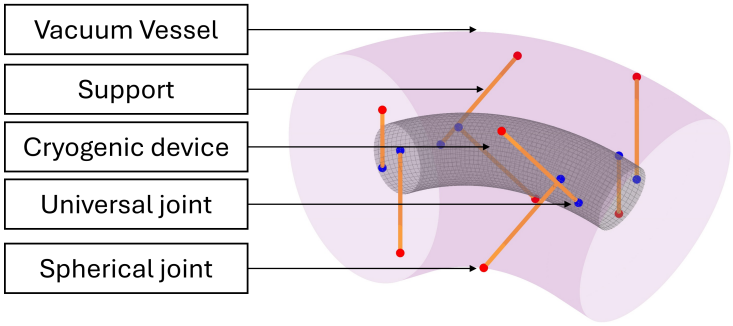

Figure 1. Cryogenic device (gray) supported by eight supports (orange) joined to it by mean of universal joints (blue) and to the vacuum vessel (pink) by mean of spherical joints (red).

The supporting system in Figure 1 is composed of n supports (a symmetric eight support architecture is shown for simplicity). Each of the $n+1$ bodies, one cold mass and n supports, has six DOFs in the 3D space, the full system has therefore $6(n+1)$ DOFs. The Model is limited to the use of spherical or a combination of spherical and universal joints at the end of each support. The choice of using only spherical and universal joints results in a support that gets loaded only axially, which makes it convenient to limit stresses and allows the designer to size a smaller cross section for the support, which, in turn, reduces the heat flux to the cold mass. The use of spherical and universal joints simplifies the model. Spherical joints lock the three translations of a body, while universal joints lock three translations and one rotation. Other combinations of different joints would introduce bending, shear, or torque in the supports. This system of joints is locking a total of $3n + 4n = 7n$ DOFs, hence the system is $n - 6$ times over-constrained. Substituting n universal joints with n spherical joints and lowering the number of DOFs locked to $6n$ does not make the system exactly constrained. This is because the n DOFs that are freed are the rotations of the supports around their longitudinal axis. The cryogenic device would still have $n - 6$ missing equations to find all reactions.

The selected and commonly used method for the solution of over-constrained systems is the Principle of virtual work [15], which equates the virtual work performed by internal actions $\mathcal{W}_{\text{int}}$ to the one performed by external reactions $\mathcal{W}_{\text{ext}}$:

$$\mathcal{W}_{\text{int}} = \mathcal{W}_{\text{ext}} \tag{1}$$

Even if, theoretically, all internal actions contribute to the work, some contributions can be eliminated because of considerations on the joints used: the only load that can generate torque, shear, and bending moments on the supports is external acceleration (in the example used is gravity). This contribution is negligible since the mass of supports is orders of magnitude smaller than the mass of the cryogenic device. All internal actions on the cryogenic device contribute minimally if the stiffness of the cryogenic device is much higher than the stiffness of the supports. The remaining actions contributing to the internal work are the eight axial actions of the supports.

The Principle of virtual work applied to over-constrained structures requires us to find a compatible exactly-constrained structure where enough constraints are substituted with

an equal number of variables. A total of $n-6$ X_m variables are introduced to eliminate the $n-6$ extra constrains resulting in the compatible structure represented in Figure 2.

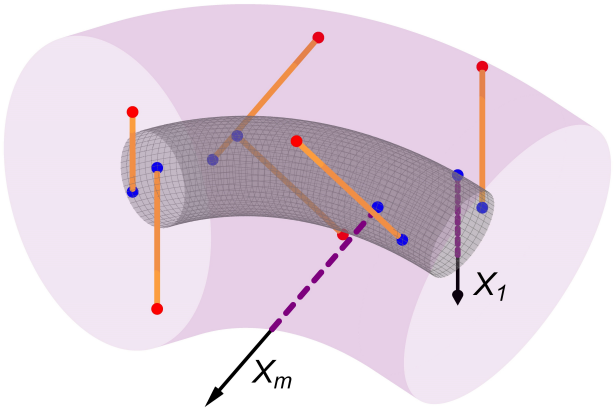

Figure 2. Compatible exactly constrained structure with over-constrained variables $X_1, \ldots, X_m$. In purple are the supports where constraints have been substituted with over-constrained variables.

The Principle of virtual work requires us to find the internal actions for $n-5$ cases of the compatible structure, as clarified in the following list:

- One compatible structure, where only external loads are applied, which is used to calculate $\mathbf{N}_0$: the vector containing internal actions on each support;
- $n-6$ compatible structures, where the over-constrained variables X_m are applied one by one as unitary loads, which are used to calculate $\mathbf{N}_{X_m}$: the vector containing the internal actions on each support.

A system of $n-6$ equations must be written to calculate all $n-6$ over-constrained variables X_m. Each equation has the form of Equation (2).

$$\sum_{i=1}^{n} \int_0^{L_i} N_{X_m,i} \left(\frac{N_{0,i} + \sum_{p=1}^{n-6} X_p N_{X_p,i}}{E_i A_i} + \frac{\delta_i}{L_i} - \frac{\delta_{P,i}}{L_i} \right) ds = \mathcal{W}_{\text{ext},X_m} \tag{2}$$

where δ and δ_P add the contributions respectively of the thermal differential contraction/expansion (see Section 2.1) and the pre-load in terms of length adjustment. Additionally, each support is described by a unique length L_i, cross section A_i and material Young Modulus E_i.

The axial actions due to over-constrained variables can be written as follows:

$$N_{X_m,i} = \begin{cases} \widetilde{N}_{X_m,i} & \text{for} \quad i = 1, \ldots, 6 \\ 1 & \text{for} \quad i = m+6 \\ 0 & \text{Otherwise} \end{cases} \tag{3}$$

all other components except for $i \leq 6$ and $i = m+6$ are null because the warm joints of respective legs in the compatible structure are not constrained axially. The i-th leg with $i = m+6$ has a unitary load derived from the Principle of virtual work solving procedure. The compatible and exactly constrained structure, which is composed of six supports, is known in robotics as a hexapod. Equations developed in robotics [16] can be used to write in a compact form equilibrium equations for the compatible structure and find the internal actions on supports:

$$\widetilde{\mathbf{N}}_{X_m} = \mathbf{J}^{-T} \mathbf{F}_m \tag{4}$$

where $\mathbf{F}_m$ is the vector containing external forces generated by a unitary load with the same application point and direction of X_m:

$$\mathbf{F}_m = (-\mathbf{w}_{m+6}, -\mathbf{u}_{m+6})^T \tag{5}$$

$\mathbf{J}$ is the geometrical Jacobian matrix [16] and can be expressed by following:

$$\mathbf{J} = \begin{bmatrix} w_{1x} & w_{1y} & w_{1z} & u_{1x} & u_{1y} & u_{1z} \\ \vdots & \vdots & \vdots & \vdots & \vdots & \vdots \\ w_{ix} & w_{iy} & w_{iz} & u_{ix} & u_{iy} & u_{iz} \\ \vdots & \vdots & \vdots & \vdots & \vdots & \vdots \\ w_{6x} & w_{6y} & w_{6z} & u_{6x} & u_{6y} & u_{6z} \end{bmatrix} \quad \text{with}$$

$$\mathbf{w}_i = \frac{{}^0\mathbf{M}_i - {}^0\mathbf{H}_i}{\|{}^0\mathbf{M}_i - {}^0\mathbf{H}_i\|} \quad \text{and} \quad \mathbf{u}_i = \mathbf{p}_i \times \mathbf{w}_i \tag{6}$$

With reference to Figure 3, $\mathbf{w}_i$ is the direction of a support element while $\mathbf{p_i}$ is the position of an arbitrary point on the support line and can be conveniently taken as $\mathbf{p}_i = \mathbf{r}_i$. Note that $\mathbf{J}$ must be calculated on the compatible exactly constrained structure.

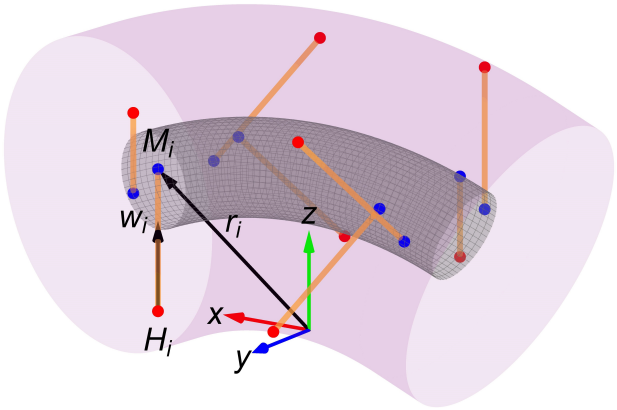

Figure 3. Scheme for the calculation of the geometrical Jacobian matrix.

Similarly, the following holds for the axial actions due to external forces:

$$N_{0,i} = \begin{cases} \widetilde{N}_{0,i} & \text{for} \quad i = 1, \ldots, 6 \\ 0 & \text{for} \quad i = 7, \ldots, n \end{cases} \tag{7}$$

with

$$\widetilde{\mathbf{N}}_0 = \mathbf{J}^{-T}\mathbf{F}_s \tag{8}$$

the external work can be written as follows:

$$\mathcal{W}_{\text{ext},X_m} = \mathbf{d} \cdot \mathbf{N}_{X_m} \tag{9}$$

where $\mathbf{d}$ is the vector containing the displacements at the warm end of each tie-rod with $d_i = -\boldsymbol{\Delta}_i \cdot \mathbf{w}_i$ its components.

The different contributions to the warm joints displacement $\boldsymbol{\Delta}_i$, which are the deformation of the vacuum vessel due to the cold mass weight, the vacuum vessel's own weight, and the pressure difference between the exterior and interior of the vessel, are introduced as follows:

$$\mathbf{\Delta}_i = \mathbf{\Delta}_{CM,i} + \mathbf{\Delta}_{OW,i} + \mathbf{\Delta}_{V,i} \tag{10}$$

where the index "CM", "OW", and "V" are used to differentiate the displacement contribution given respectively by the cold mass weight, the weight of the vacuum vessel, and the vacuum. The different terms of the warm joints displacement are calculated as follows:

$$\Delta_{CM,il} = D_{CM,ilk}\left(N_0^k + \sum_{p=1}^{n-6} X_p N_{X_p}^k\right) \tag{11}$$

$$\Delta_{OW,il} = D_{OW,ilk} F_g^k \tag{12}$$

with $\mathbf{F}_g = (Cos(\theta), Sin(\theta))$ the direction of gravity supposing the device rotates of θ from a vertical position. $\mathbf{\Delta}_{V,i}$ is measured directly from FEAs while the compliance matrices D_{ilk} are defined in the same way as in the model developed by these same authors for an exactly constrained system [17].

Once all X_m are known, the Principle of virtual work can be applied again to extract the pose (position and rotation) $\mathbf{e} = (e_x, e_y, e_z, \theta_x, \theta_y, \theta_z)$ of the cryogenic device by solving six independent equations of the form: Equation (13). Each equation requires us to calculate the internal actions $\mathbf{N}_j$ on each support when a unitary force/torque is applied to the compatible structure.

$$\sum_{i=1}^{n} \int_0^{L_i} N_{j,i}\left(\frac{N_{0,i} + \sum_{p=1}^{n-6} X_p N_{X_p,i}}{E_i A_i} + \frac{\delta_i}{L_i} - \frac{\delta_{P,i}}{L_i}\right) ds = \mathbf{d} \cdot \mathbf{N}_j + e_j = \mathcal{W}_{\text{ext},j} \tag{13}$$

where the internal actions $\mathbf{N}_j$ used for the calculation of the pose are found as follows:

$$N_{j,i} = \begin{cases} \widetilde{N}_{j,i} & \text{for} \quad i = 1, \ldots, 6 \\ 0 & \text{for} \quad i = 7, \ldots, n \end{cases} \tag{14}$$

and

$$\widetilde{\mathbf{N}}_j = \mathbf{J}^{-T} \mathbf{F}_j \tag{15}$$

where $\mathbf{F}_{j,i} = 1$ for $i = j$ and 0 otherwise.

An example implementation of the code in Wolfram Mathematica is given in Appendix B.

2.1. Influence of the Differential Thermal Contraction

The thermal contraction of the cold mass and of the supports is introduced as a virtual internal strain on the supports $\varepsilon_T = \delta / L$. The thermal expansion δ originates from two contributions: the contraction of the cold mass δ_{CM} and the contraction of the support δ_s

$$\delta = \delta_{CM} + \delta_s \tag{16}$$

Because the coefficient of linear expansion depends on the temperature, the integral form of the coefficient is used to obtain the length of a rod at a given temperature L_T:

$$L_T - L_{293} = I(T) L_{293} \tag{17}$$

The function of $I(T)$ for different material can be found on [18]. This is, however, the case of a rod that is initially at temperature $T = 293\,\text{K}$ and is cooled homogeneously at a given temperature T. In the study case, this is not valid as there is a strong temperature

gradient along the length of the supports where the cold end is at around 5 K and the warm end at 293 K. Thus, an integral form of Equation (17) must be used:

$$\delta_s = \int_0^L I(T(s))\, ds \tag{18}$$

The temperature along the length L of a rod with its extremities at temperatures T_0 and T_L can be found by solving the differential equations of Fourier's law:

$$\frac{\partial}{\partial s}\left(k\frac{\partial T}{\partial s}\right) + \dot{q} = \rho c \frac{\partial T}{\partial t} \tag{19}$$

supposing the steady state $\dfrac{\partial T}{\partial t} = 0$ and that there are no heat sources within the support $\dot{q} = 0$, Fourier's law becomes:

$$\frac{\partial k}{\partial T}\left(\frac{\partial T}{\partial s}\right)^2 + k\frac{\partial^2 T}{\partial^2 s} = 0 \tag{20}$$

where $k = k(T)$. Looking at the thermal conductivity of the possible materials for supports [18] their thermal conductivity appears to be proportional to $\sqrt{T}$ so that $k \simeq a\sqrt{T}$. Substituting in Equation (20) and solving the differential equations with boundary conditions $T(0) = T_0$ and $T(L) = T_L$ yields the following:

$$T(s) = \left(-\frac{LT_0^{\frac{2}{3}} - T_0^{\frac{2}{3}}s + T_L^{\frac{2}{3}}s}{L}\right)^{\frac{2}{3}} \tag{21}$$

The real function $T(s)$ is written in a piece-wise form because of the presence of an intermediate thermalization T_{th} of length L_{th} between the warm T_a and cold T_c parts of the support of lengths L_w and L_c, respectively:

$$T(s) = \begin{cases} \left(-\dfrac{L_w T_a^{\frac{2}{3}} - T_a^{\frac{2}{3}}s + T_{th}^{\frac{2}{3}}s}{L_w}\right)^{\frac{2}{3}} & \text{for} \quad 0 \le s < L_w \\ T_t h & \text{for} \quad L_w \le s < L_w + L_{th} \\ \left(-\dfrac{L_w T_{th}^{\frac{2}{3}} - T_{th}^{\frac{2}{3}}(s - L_w - L_{th}) + T_c^{\frac{2}{3}}(s - L_w - L_{th})}{L_c}\right)^{\frac{2}{3}} & \text{for} \quad L_w + L_{th} \le s \le L \end{cases} \tag{22}$$

Codes of numerical integration can be used to integrate Equation (18) with Equation (22) to obtain δ_s.

If the contraction of the support and the contraction of the cold mass are in opposite directions, then, due to the contraction of the cold mass, a support of nominal length should stretch even more for the system to be in equilibrium. In equilibrium $L_e = \|{}^0\mathbf{M}_{i,c} - {}^0\mathbf{H}_i\|$, where $\mathbf{M}_{i,c}$ is the i-th cold joint position at the cold mass. In order to have a coherent math $\delta_{CM} = L - L_e$, so that $\delta_{CM} + \delta_s$ represents the total elongation that the support should reach in equilibrium. Even if the contractions are in the same direction, the math is coherent with this sign convention. The cold joint position at cold is calculated as follows $\mathbf{M}_{i,c} = \mathbf{M}_i I(T_c)$.

2.2. Limitations of the Model

The model presented is limited to the calculation of axial internal actions only on the supports, that must be joined to the vacuum vessel and the cold mass either by spherical joints or one spherical joint and one universal joint. Although the model is capable of

estimating compression loads and can be used not only for tie rods but also struts resisting compression, instability phenomena such as buckling must be checked. In case of instability, the displacements predicted by the model will not match the case studied.

3. Validation of the LPM

The LPM has been particularized to three study cases:

- An eight support arrangement for a generic device;
- An eleven support arrangement for a generic device;
- A possible application of an eight support arrangement for a superconducting dipole with an application in the medical field of Hadron-therapy [19,20] is given in Appendix C.

The particularized LPM has been validated by FEA by mean of *Ansys® Workbench, 2022 R2*. Linear static thermo-mechanical analysis has been simulated. The materials used and loads applied and the boundary conditions of the model are explained in the following paragraphs:

- **Geometry:**
  Eight or eleven supports constitute the supporting system of a generic cryogenic device Figure 4. The supports connect the cold mass to the external vacuum vessel. The disposition of supports has been randomly generated to prove that the mathematical model developed can be adapted to non-symmetrical configurations too. Eleven has been chosen as an arbitrary number greater than eight (one of the most common supporting architecture [3]).

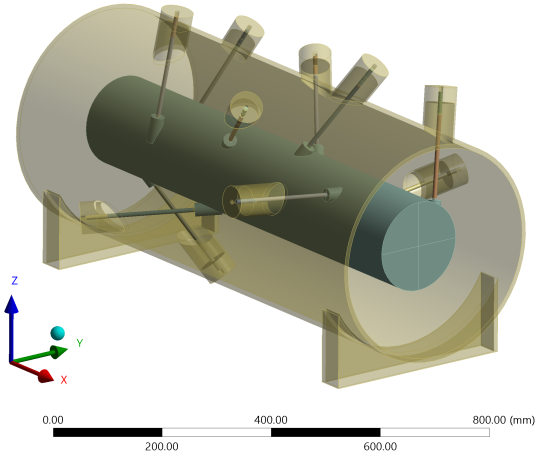

Figure 4. Model used for the validation of the LPM. Eleven supporting rods attached to the vacuum vessel and the cold mass. The model used for the validation of eight supports is the same as for the eleven rods with three random rods suppressed. Images used courtesy of ANSYS, Inc.

- **Material**:
  Temperature dependent coefficient of thermal expansion and thermal conductivity of Stainless steel 304 [18] are being used to define the properties of the steel material applied to supporting elements.
- **Interactions**
  Spherical joints and bushing joints (general Ansys joints defined by stiffness parameters) have been used to simulate the joints between the supports and the vacuum vessel or supports and cold mass. Both types of joints have been scoped to single nodes on the surfaces of the bodies to join (see Figure 5). A short section of supports acts as a stiffener (see Figure 5). This section is assigned with a 1000 times stiffer custom steel; it

prevents the elements near the nodes scoped for the joints from deforming excessively. Bushings are used to formulate a universal joint by defining the stiffness associated with the degrees of freedom to lock between the nodes, a value of $1 \times 10^9\,\mathrm{N\,mm^{-1}}$ is assigned to stiffen the relative translations along x, y, and z (longitudinal axis of the supports), and a value of $1 \times 10^9\,\mathrm{N\,mm/deg}$ is assigned to the stiffness of rotations around z.

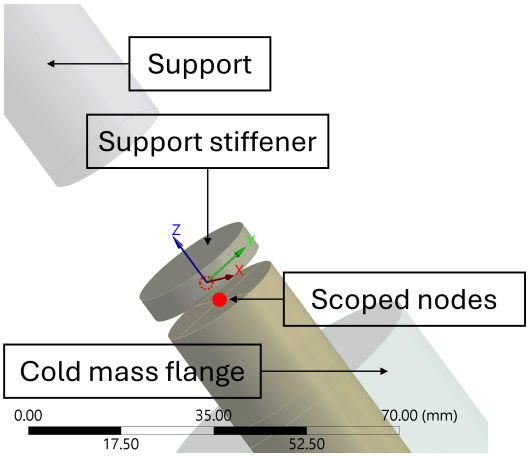

Figure 5. Support stiffeners section and joint definition in ANSYS. Images used courtesy of ANSYS, Inc.

- **Loads**
  To validate the general validity of the model, six different loading conditions have been applied in this simulation: forces F_x, F_y, F_z and moments M_x, M_y, M_z are applied separately in each of the six steps (Table 1). The vacuum of -0.1 MPa is applied to the vacuum vessel's internal surfaces. Pre-load has been applied by defining translation joints and applying joint load as displacement ($\delta = 0.5$ mm). Both vacuum and pre-load are applied before step 1 together with Temperature stationary boundary conditions of 22 °C on the vacuum vessel and -268 °C on the cold mass.

Table 1. Loading conditions for the validation models.

Step	F_x kN	F_y kN	F_z kN	M_x kN m	M_y kN m	M_z kN m
1	5	0	0	0	0	0
2	0	5	0	0	0	0
3	0	0	5	0	0	0
4	0	0	0	0.4	0	0
5	0	0	0	0	2	0
6	0	0	0	0	0	2

Note that M_x is five times lower than other applied moments because otherwise, one support would buckle under compression, rendering the results of the FEAs and LPM drastically different. Given that the scope of this model is not to assess the position of a cryogenic device with supports in buckling conditions, the validation is not impacted.

4. Results and Discussion

The evaluation of the accuracy of the pose (position and rotation) of cryogenic elements and internal actions on supporting elements is of paramount importance to assess the structural integrity and performance of machines operating at cryogenic temperatures. In this section, we report the comparison of results of internal actions and pose as calculated by the developed LPM model, which is benchmarked against FEA (simulation options described in Section 3).

Internal actions on supports are calculated from LPM using $N_{0,i} + \sum_{m=1}^{n-6} X_m N_{X_m,i}$; the values of all over-constrained variables X_m are calculated from Equation (2). The same internal actions are evaluated from FEA by probing joint loads. As mentioned in Table 1, loads are applied in six different steps of the simulation. The values calculated with the LPM are in good agreement with those simulated by FEAs for both the eight and eleven support study cases (Figure 6).

Tables 2 and 3 report values of internal axial load on each support for each loading case simulated with FEA. Additionally, figures of merit such as the absolute error Err = LPM − FEA and relative error %Err = |Err|/FEA ∗ 100 are calculated to express the accuracy of the developed model with respect to FEA. The maximum absolute error found is relatively low, about 360 N and 400 N if compared to a maximum force of 37 kN and 51 kN respectively for the eight and eleven supports study cases. Maximum absolute errors occur for high values of the internal actions; therefore, the relative error is relatively small. High relative errors (%Err = |Err|/FEA ∗ 100) can be found for those supports that are minimally loaded; for example, on the seventh rod of the eight support supporting system for the sixth load case. The two models, in this particular case, disagree by only 52 N in absolute terms. The axial load is around 100 N for that support; thus, the relative error is high. The same issue is highlighted for the eleven support supporting system (Table 3). In this case rod 3 shows a very small disagreement of 7 N but on a nominal value of about 14 N, consequently the relative error is high. While sizing supports, the engineering focus is more on the maximally loaded supports, where the model shows lower relative errors. An overall figure of merit chosen to describe the accuracy of the model is, therefore, the median of all relative errors (used from now on), which is about 1.1% and 1.4% respectively for the eight and eleven support study case. This quantitatively confirms the very good agreement of the model with FEAs. Although the accuracy slightly decreases with a larger number of rods, the model can be judged as reliable.

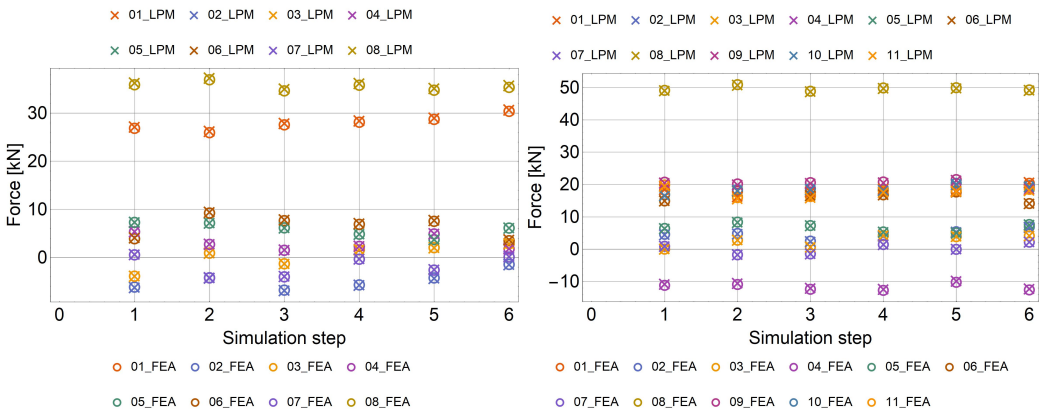

(**a**) Eight supports. (**b**) Eleven supports.

Figure 6. Comparison of the force on each support between the LPM (cross) and FEA (circle).

The pose of the suspended cryogenic device has been calculated by means of the LPM. The qualitative agreement with the LPM is reported in Figure 7. Tables 4 and 5 report the values of all pose components for each loading case (see Table 1) as simulated by FEAs. Similarly, as was performed for the axial force, the same tables report the absolute error Err and relative error %Err. The maximum absolute error between the two models in estimating the position of the suspended object is 13 µm and 26 µm, while for rotations is 52 µrad and 99 µrad. For the pose, there is the same issue in estimating the overall accuracy of the model as for the internal actions. Specifically, a high relative error is shown for d_y during the sixth load case in Table 5. Here, the absolute disagreement between the two models is very low: about 2 µm for a nominal value of 10 µm thus the high relative error.

In a real application, displacements so small are fully within the required accuracy of the system (order of 0.1–0.3 mm and 0.1–0.3 mrad) and are even outside of the sensitivity of measurement instruments. Therefore, it has been chosen to characterize the accuracy of the model again with the median of all relative errors calculated. Even though some high errors appear in particular cases, the median of all errors is only about 0.6% and 1.4% respectively for the eight and eleven support study cases, confirming for the pose a very good agreement of the developed model with FEAs. The accuracy slightly decreases for the model with eleven supports but is still accurate enough to be used in optimization processes, the comparison of different material and dimensional solutions, and sensitivity analysis.

Table 2. Absolute and relative errors of internal actions on each support for the eight support study case.

	Step	**Rod 1**	**Rod 2**	**Rod 3**	**Rod 4**	**Rod 5**	**Rod 6**	**Rod 7**	**Rod 8**
FEA (kN)	1	26.8	−6.2	−3.9	5.4	7.3	3.9	0.6	35.9
	2	25.9	−4.2	0.9	2.7	7.2	9.2	−4.3	36.9
	3	27.6	−6.8	−1.3	1.5	6.1	7.6	−4.0	34.6
	4	28.1	−5.7	1.6	2.3	4.8	6.9	−0.4	35.8
	5	28.7	−4.3	2.0	4.9	3.7	7.5	−2.6	34.8
	6	30.4	−1.4	2.9	1.8	6.1	3.5	0.1	35.4
Err (N)	1	274.9	−79.6	0.7	21.2	−2.5	176	43	360
	2	271	−75.3	−33.6	42.7	−10.2	173.5	62	352.4
	3	273.5	−74.9	−28.2	41.5	−3.2	166.7	54.2	357.9
	4	265	−76.7	−6.8	24.6	−6	172.7	47.5	347
	5	269.6	−75.1	−21.9	35.4	−4.8	168.5	52.6	350.9
	6	273.5	−78.4	−13.6	26	−7.2	177.7	51.6	350.6
% Err	1	1	1.3	0	0.4	0	4.5	7.6	1
	2	1	1.8	3.7	1.6	0.1	1.9	1.5	1
	3	1	1.1	2.2	2.8	0.1	2.2	1.4	1
	4	0.9	1.3	0.4	1.1	0.1	2.5	13.3	1
	5	0.9	1.8	1.1	0.7	0.1	2.2	2	1
	6	0.9	5.5	0.5	1.5	0.1	5.1	61.9	1

The validation highlights the ability of the model to correctly estimate interesting quantities such as loads and position of objects in a general way. The validation proves the effectiveness of the model in predicting those quantities, even for support configurations that are highly non-symmetrical.

Computational performances and system information are reported in Table 6 to facilitate reproducibility of results. The same machine has been used to run both LPMs and FEAs using respectively Wolfram Mathematica and Ansys. The solution time by means of the developed LPM code shows an improvement of about 130 times with respect to currently widely used FEA software. Although the time cost of a single simulation of 144 s does not seem to justify the use of the mathematical model, optimization algorithms based on the mathematical model can highly benefit from the time reduction. For example, an optimization that analyzes 100,000 different configurations of 11 supports would take 2 days for the mathematical code and about 200 days for a classical FEA approach. Additionally, the mathematical model developed represents a way of crosschecking results of FEA simulations that can be highly influenced by wrongly chosen simulation options and boundary conditions.

Table 3. Absolute and relative errors of internal actions on each support for the eleven support study case.

	Step	Rod 1	Rod 2	Rod 3	Rod 4	Rod 5	Rod 6	Rod 7	Rod 8	Rod 9	Rod 10	Rod 11
FEA (kN)	1	18.2	4.6	0.0	−11.2	6.4	14.9	0.9	49.1	20.7	16.9	19.9
	2	16.0	4.9	2.7	−10.9	8.3	18.0	−1.8	50.9	20.1	18.5	15.9
	3	17.5	2.5	0.6	−12.4	7.3	16.6	−1.5	48.8	20.6	18.7	16.2
	4	18.4	4.2	4.2	−12.7	5.3	16.8	1.4	49.9	20.8	18.5	17.9
	5	17.9	5.4	3.9	−10.2	5.1	17.6	0.0	49.9	21.5	20.4	18.2
	6	20.4	6.9	4.1	−12.6	7.6	14.1	2.2	49.3	18.8	19.6	18.5
Err (N)	1	177.4	−172.7	7.1	304.7	−75.2	−14	−7.5	−160.4	−296	−348	−377.3
	2	183	−160.6	13.9	308.5	−92.4	−11.9	−2.5	−179.2	−296.1	−364.4	−382.4
	3	174.3	−171.8	6.5	310.3	−64.1	−9.7	−0.9	−145.2	−292.7	−328.6	−374.5
	4	177.9	−168.9	26.1	301.7	−84.6	−11.7	−14.6	−184.1	−304.3	−363	−383.3
	5	178.3	−160.8	24.1	307.8	−92	−5.6	−13.4	−192.2	−300.6	−368.3	−383.8
	6	188.4	−158.2	40.4	296.3	−97.2	−11.7	−15.6	−191.9	−298.9	−376.6	−393.3
% Err	1	1	3.8	51.4	2.7	1.2	0.1	0.8	0.3	1.4	2.1	1.9
	2	1.1	3.3	0.5	2.8	1.1	0.1	0.1	0.4	1.5	2	2.4
	3	1	6.9	1	2.5	0.9	0.1	0.1	0.3	1.4	1.8	2.3
	4	1	4.1	0.6	2.4	1.6	0.1	1	0.4	1.5	2	2.1
	5	1	3	0.6	3	1.8	0	34.8	0.4	1.4	1.8	2.1
	6	0.9	2.3	1	2.3	1.3	0.1	0.7	0.4	1.6	1.9	2.1

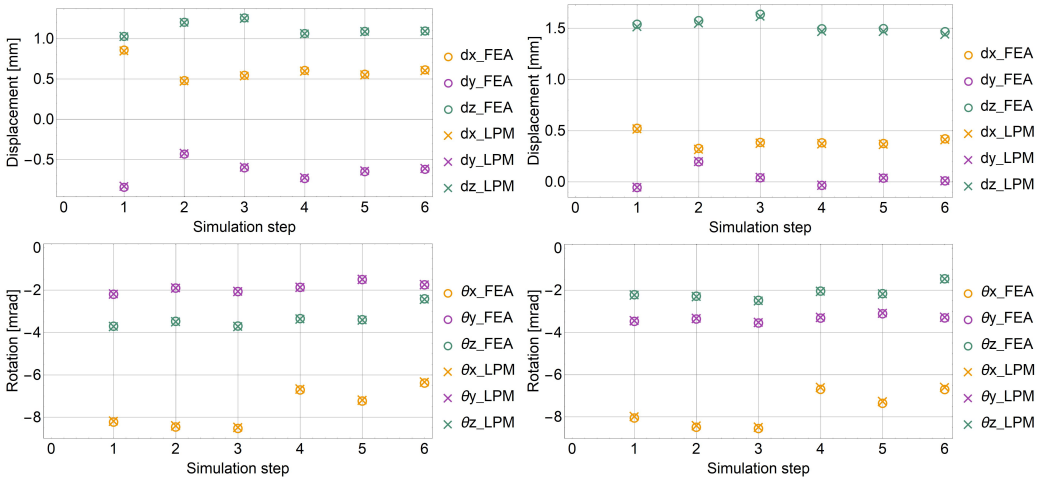

(**a**) Eight supports. (**b**) Eleven supports.

Figure 7. Comparison of the pose (displacement and rotation) of the cold mass between the LPM (cross) and FEA (circle).

Table 4. Errors for each DOF for the model with eight supports.

	Step	dx mm	dy mm	dz mm	θx mrad	θy mrad	θz mrad
FEA	1	0.86	−0.84	1.03	−8.23	−2.19	−3.7
	2	0.48	−0.43	1.2	−8.46	−1.91	−3.48
	3	0.55	−0.6	1.26	−8.53	−2.07	−3.7
	4	0.61	−0.74	1.06	−6.72	−1.88	−3.35
	5	0.56	−0.65	1.09	−7.24	−1.5	−3.39
	6	0.61	−0.62	1.09	−6.39	−1.75	−2.42

Table 4. *Cont.*

	Step	dx mm	dy mm	dz mm	θx mrad	θy mrad	θz mrad
Err	1	−0.011	0.013	−0.001	0.045	0.01	−0.016
	2	−0.007	0.009	−0.004	0.052	0.006	−0.019
	3	−0.007	0.01	−0.004	0.051	0.008	−0.017
	4	−0.009	0.012	−0.002	0.046	0.007	−0.016
	5	−0.008	0.011	−0.002	0.046	0.004	−0.017
	6	−0.008	0.01	−0.003	0.048	0.006	−0.02
% Err	1	1.2	1.6	0.1	0.6	0.5	0.4
	2	1.4	2	0.3	0.6	0.3	0.5
	3	1.4	1.6	0.3	0.6	0.4	0.5
	4	1.4	1.6	0.2	0.7	0.4	0.5
	5	1.4	1.7	0.2	0.6	0.3	0.5
	6	1.4	1.7	0.2	0.8	0.4	0.8

Table 5. Errors for each DOF for the model with eleven supports.

	Step	dx mm	dy mm	dz mm	θx mrad	θy mrad	θz mrad
FEA	1	0.52	−0.06	1.54	−8.06	−3.47	−2.21
	2	0.33	0.2	1.57	−8.49	−3.37	−2.29
	3	0.38	0.04	1.64	−8.56	−3.55	−2.48
	4	0.38	−0.04	1.49	−6.7	−3.32	−2.04
	5	0.37	0.04	1.5	−7.36	−3.12	−2.16
	6	0.42	0.01	1.47	−6.7	−3.31	−1.46
Err	1	−0.008	0.002	−0.024	0.071	0.028	−0.018
	2	−0.009	0.004	−0.024	0.072	0.032	−0.017
	3	−0.008	0.003	−0.021	0.063	0.026	−0.022
	4	−0.009	0.002	−0.025	0.092	0.03	−0.014
	5	−0.009	0.003	−0.026	0.085	0.035	−0.015
	6	−0.009	0.002	−0.026	0.099	0.031	−0.007
% Err	1	1.4	3.7	1.6	0.9	0.8	0.8
	2	2.8	2	1.5	0.8	0.9	0.7
	3	2.1	8.9	1.3	0.7	0.7	0.9
	4	2.3	6.6	1.6	1.4	0.9	0.7
	5	2.5	9	1.8	1.2	1.1	0.7
	6	2.2	24.1	1.8	1.5	0.9	0.5

Table 6. System information and simulation time performances of the FEA and LPM.

OS Name	Microsoft Windows 10 Pro			
Version	10.0.19045 Build 19045			
System Model	HP Z4 G4 Workstation			
Processor	Intel(R) Xeon(R) W-2155 CPU @ 3.30 GHz, 3312 Mhz, 10 Core(s), 20 Logical Processor(s)			
RAM	64.0 GB			
Study case	8 supports		11 supports	
Program	Ansys 2022 R2 Build 22.2	Wolfram Mathematica 13.0	Ansys 2022 R2 Build 22.2	Wolfram Mathematica 13.0
Nodes	250,000		301,000	
Elements	72,000		141,000	
Time	144 s	1.1 s	177 s	1.19 s
RAM used	7.6 GB		9.32 GB	
Cores used	10		10	

5. Conclusions

This work proposed a generic semi-analytical model (LPM) of the supporting system of a cryogenic device supported by any number of tie rods (rods with spherical joints at each end or one spherical and one universal joint), in order to better structure and formalize the analysis of supporting systems for this application. The model enables us to calculate the internal loads for all supports and the displacement (all six DOF) of the cryogenic device as an effect of the combination of a generic external load $(F_x, F_y, F_z, M_x, M_y, M_z)$, pre-load on each support, vacuum and thermal contraction due to cool-down, thus filling

the knowledge gap of existing models either limited by the geometrical constrains or the lack of assessment for the effect of thermal contraction.

Two study cases of the model for a support architecture of eight and eleven tie-rods have been validated against the results obtained with a standard and acknowledged finite element analysis (FEA) software running linear thermal–mechanical simulations. The model in both study cases reproduce FEA results with a median relative error of 1.4%, proving its efficacy in reproducing the results of standard software. The accuracy slightly decreases, resulting in median relative error from 1.1% to 1.4%, with the increase in tie-rods in the support architecture. Such results have been obtained for randomly arranged tie-rods, which proves the validity of the model even for geometries that lack symmetry.

The model proposed in this work produces, in a computationally cheaper way, results that are in strong agreement with those calculated by a popular and acknowledged software for FEA. The run-time for a single run of the same simulation is 130 times faster than FEAs run on the same machine. This is a considerable advantage especially in optimization routines where months of FEAs can be transformed into days or hours.

This model opens the possibility for designers to run extensive and effective optimization routines while searching through a wide solution space, which results from the combination of material, dimensions and arrangement of supports. Additionally, the model enables us to run computationally cheaper and more comprehensive sensitivity analysis, which helps us to better grasp the interplay of input parameters and desired outputs.

Author Contributions: Conceptualization L.P., L.D., D.P., A.R. and S.U. Formal analysis, L.P.; Investigation, L.P.; Methodology, L.P. and L.D.; Visualization, L.P.; Writing—original draft, L.P.; Writing—review and editing, L.D., D.P., A.R., T.T. and S.U.; Supervision, L.D., D.P. and S.U.; Project administration, L.D., D.P., A.R., T.T. and S.U.; Funding acquisition, T.T. All authors have read and agreed to the published version of the manuscript.

Funding: This project has received funding from the European Union's Horizon 2020 Research and Innovation programme under HITRIplus grant agreement No 101008548. This study has received support from the CERN Budget for Knowledge Transfer to Medical Applications, in the frame of the Next Ion Medical Machine Study. This work has been supported by the EU Recovery and Resilience Facility within the Project No 5.2.1.1.i.0/2/24/I/CFLA/003 "Implementation of consolidation and management changes at Riga Technical University, Liepaja University, Rezekne Academy of Technology, Latvian Maritime Academy and Liepaja Maritime College for the progress toward excellence in higher education, science and innovation" academic career doctoral grant (ID 1026).

Institutional Review Board Statement: Not applicable.

Informed Consent Statement: Not applicable.

Data Availability Statement: Data are contained within the article.

Conflicts of Interest: The authors declare no conflicts of interest.

Abbreviations

The following abbreviations are used in this manuscript:

DOF	Degrees of Freedom
FEA	finite element analysis
LPM	lumped parameter model

Appendix A. Particularization of LPM to Eight Supports

For the particular case of the LPM for a support architecture that uses eight equal supports, the system is twice over-constrained. A system of two equations (equal to the number of over-constrained variables unknown) is written to solve for X and Y (Equation (A1)).

$$\begin{cases} \int_0^L \mathbf{N}_X \cdot \left(\dfrac{\mathbf{N}_0 + X\mathbf{N}_X + Y\mathbf{N}_Y}{EA} + \dfrac{\delta}{L} - \dfrac{\delta_P}{L} \right) ds = \mathcal{W}_{\text{ext},X} \\ \int_0^L \mathbf{N}_Y \cdot \left(\dfrac{\mathbf{N}_0 + X\mathbf{N}_X + Y\mathbf{N}_Y}{EA} + \dfrac{\delta}{L} - \dfrac{\delta_P}{L} \right) ds = \mathcal{W}_{\text{ext},Y} \end{cases} \tag{A1}$$

The internal actions $\mathbf{N}_0$ given by an external load are calculated as follows:

$$N_{0i} = \begin{cases} \widetilde{N}_{0i} & \text{for} \quad i = 1, \ldots, 6 \\ 0 & \text{for} \quad i = 7, 8 \end{cases} \tag{A2}$$

where $\widetilde{\mathbf{N}}_0 = \mathbf{J}^{-T}\mathbf{F}_s$

Similarly, the axial reactions are written for the two virtual structures where each hyperstatic virtual load is applied:

$$N_{Xi} = \begin{cases} \widetilde{N}_{Xi} & \text{for} \quad i = 1, \ldots, 6 \\ 1 & \text{for} \quad i = 7 \\ 0 & \text{for} \quad i = 8 \end{cases} \tag{A3}$$

and

$$N_{Yi} = \begin{cases} \widetilde{N}_{Yi} & \text{for} \quad i = 1, \ldots, 6 \\ 0 & \text{for} \quad i = 7 \\ 1 & \text{for} \quad i = 8 \end{cases} \tag{A4}$$

where

$$\widetilde{\mathbf{N}}_X = \mathbf{J}^{-T}\mathbf{F}_{Xs} \quad \text{and} \quad \mathbf{F}_{Xs} = (-\mathbf{w}_7, -\mathbf{u}_7)^T$$

$$\widetilde{\mathbf{N}}_Y = \mathbf{J}^{-T}\mathbf{F}_{Ys} \quad \text{and} \quad \mathbf{F}_{Ys} = (-\mathbf{w}_8, -\mathbf{u}_8)^T$$

Once X and Y are known, the Principle of virtual work can be applied to extract the pose (position and rotation) $\mathbf{e} = (e_x, e_y, e_z, \theta_x, \theta_y, \theta_z)$ of the cryogenic device by solving six independent equations of the form: Equation (A5).

$$\int_0^L \mathbf{N}_j \cdot \left(\frac{\mathbf{N}_0 + X\mathbf{N}_X + Y\mathbf{N}_Y}{EA} + \frac{\delta}{L} - \frac{\delta_P}{L} \right) ds = \mathcal{W}_{\text{ext},j} \tag{A5}$$

the internal actions used for the calculation of the pose are found as follows:

$$N_{j,i} = \begin{cases} \widetilde{N}_{j,i} & \text{for} \quad i = 1, \ldots, 6 \\ 0 & \text{for} \quad i = 7, 8 \end{cases} \tag{A6}$$

and

$$\widetilde{\mathbf{N}}_j = \mathbf{J}^{-T}\mathbf{F}_j \tag{A7}$$

where $\mathbf{F}_{j,i} = 1$ for $i = j$ and 0 otherwise.

Appendix B. Code Example

An example of the code programmed in Wolfram Mathematica 13.0 is given below. This code provides only a basic example of the implementation of the code to obtain the axial loads on each support and displacements of the suspended object given the external loads $(F_x, F_y, F_z, M_x, M_y, M_z)$, the pre-load δ_P in mm. The matrices governing the

deformation of the vacuum vessel D_{cm}, D_{ow}, D_v appear as variables, and their calculation is explained in [17]. The calculation of the thermal contraction δ is left to the reader following Equation (16).

```
(*number of tie rods*)
n = 11;
(*example of a 11 tie-rods geometry*)
geometry = {{{-184.1, 48.4, -87.5}, {-112.6, 173.4, -129.4}}, {{267.9, -75.8,
    65.2}, {260.2, -224.6, 82.6}}, {{108.9, 4.1, 99.9}, {178.8, 59.9, 220.3}},
    {{387.2, 83.2, 55.4}, {346.6, 124., 193.9}}, {{-360.8, 98.1, 19.5}, {-296.,
    138.5, 148.6}}, {{-48.5, -57.4, 81.9}, {60.7, -113.5, 168.1}}, {{-254.7,
    -67.7, 73.6}, {-234.6, -51.9, 221.4}}, {{-155.7, -56.8, -82.3}, {-243.1,
    -178.2, -93.5}}, {{147.,95.7, -29.}, {173.2, 239.3, 5.5}}, {{-361.4, 5.9,
    -99.8}, {-294., 68.1, -218.5}}, {{38.5, 77., 63.8}, {-58.1, 145.7, 155.8}}}
(*geometry of the compatible structure*)
ISOgeometry = Drop[geometry, -(n-6)];
directionM = Table[Normalize[Geometry[[i, 2]] - Geometry[[i, 1]]], {i, 1, n}];
(*input external forces components*)
Fs = {Fx, Fy, Fz, Mx, My, Mz};
(*calculates the forces for each support in the compatible structure*)
N0 = Join[Transpose[J[ISOgeometry]].Fs, ConstantArray[0, n - 6]];
(*calculates w_i*)
w = Table[Normalize[geometry[[i]][[2]] - geometry[[i]][[1]]], {i, 7, n}];
(*calculates u_i*)
u = Table[Cross[geometry[[i]][[1]], Normalize[geometry[[i]][[2]] - geometry[[i
    ]][[1]]]], {i, 7, n}];
Fm = Join[#[[1]], #[[2]]] & /@ Transpose[{w, u}];
(*support internal actions due to application of unitary loads due to over-
    constrain variables*)
NXm = Table[Join[Transpose[J[ISOgeometry]].Fm[[i]], IdentityMatrix[n-6][[i]]], {i,
     1, n-6}];
(*over-constrain variables*)
X = {X1, X2, X3, X4, X5};
(*Equation (2)*)
eq = Table[Nv[[j]].(N0 + X.NXm + δ RodStiffness - δP) == RodStiffness*Table[(Dcm.(
    N0 + X.NXm))[[i]].directionM[[i]], {i, 1, n}].NXm[[j]] + RodStiffness*Table[(
    Dow.{Cos[ang], Sin[ang]})[[i]].directionM[[i]], {i, 1, n}].NXm[[j]] +
    RodStiffness*Table[Dv[[i]].directionM[[i]], {i, 1, n}].NXm[[j]], {j, 1, n
    -6}];
(*solves the system of equations calculating the over-constrain variables*)
sol = NSolve[eq, X];
localX = X /. sol[[1]];
(*calculates internal actions on the real structure*)
forces = N0 + localX.NXm;
(*calculates disaplacements of the supported device Equation (13)*)
displcement = Table[1/RodStiffness*Join[Transpose[J[ISOgeometry]].IdentityMatrix
    [6][[j]], ConstantArray[0, n-6]].(N0 + localX.NXm + δ RodStiffness - δP) -
    Join[Transpose[J[ISOgeometry]].IdentityMatrix[6][[j]], ConstantArray[0, n
    -6]].Table[(Dcm.(N0 + localX.NXm)[[i]].directionM[[i]], {i, 1, n}] - Join[
    Transpose[J[ISOgeometry]].IdentityMatrix[6][[j]], ConstantArray[0, n-6]].
    Table[(Dow.{Cos[ang], Sin[ang]})[[i]].directionM[[i]], {i, 1, n}] - Join[
    Transpose[J[ISOgeometry]].IdentityMatrix[6][[j]], ConstantArray[0, n-6]].
    Table[Dv[[i]].directionM[[i]], {i, 1, n}], {j, 1, 6}];
```

Appendix C. Real Application Example

Ion therapy is an established treatment for cancer. The beam necessary for treatment is generated from ion sources and is accelerated either in a cyclotron or synchrotron to then be delivered to the patient through the so-called "transfer line". The transfer line can be fixed horizontally, fixed vertically, or can rotate. In the last case, a robust machine called "gantry" is necessary to support the transfer line during rotation (Figure A1).

The implementation of superconducting technologies to steer the beam allows for a reduction in the size of the system. However, the implementation of superconducting technologies on a rotating machine is much more complex than the normal-conducting counterpart. The supporting system of superconducting magnets must operate in a vacuum and cryogenic environment in addition to the high cycle fatigue environment due to the rotation of the machine.

The model proposed in this article can be used to support design decisions on the best arrangement and material for supports to minimize displacements during the rotation of the machine, which can negatively affect the treatment.

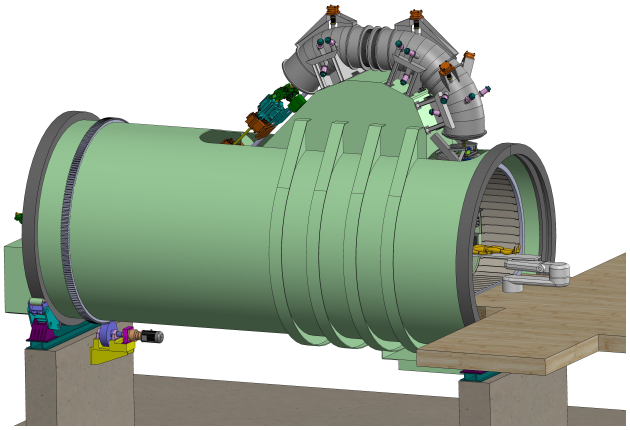

Figure A1. Overall 3D assembly of a proposed superconducting carbon ion gantry first analyzed in [17].

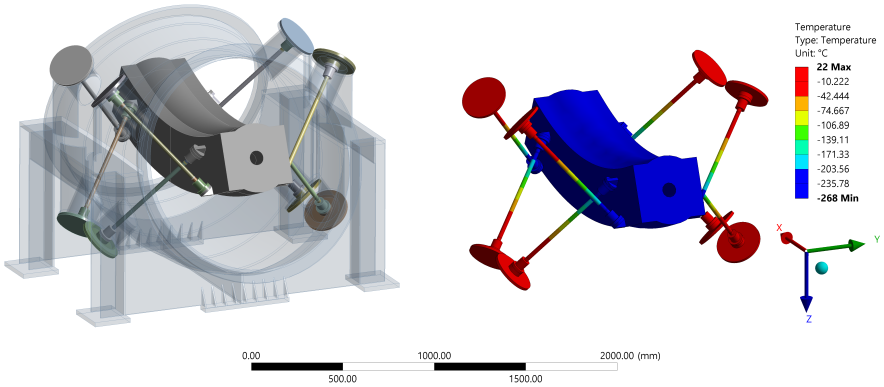

Figure A2. Model used for the validation of the LPM. Distribution of temperature from the steady state thermal analysis. Images used courtesy of ANSYS, Inc.

Appendix C.1. Problem Description

- **Geometry**:
  Eight supports support the superconducting dipole inside the vacuum vessel (Figure A2). The supports are positioned in a symmetric way in order to have a self-aligning contraction of the system. Each support is connected to the vacuum vessel and to the cold mass, respectively, by a spherical joint and a universal joint.
- **Material**:
  Temperature dependent coefficient of thermal expansion and thermal conductivity of Stainless steel 304 [18] are being used to define the properties of the steel material applied to supporting elements.
- **Interactions**
  Spherical joints and bushing joints (general Ansys joints defined by stiffness parameters) have been used to simulate the joints between the supports and the vacuum

vessel or supports and cold mass. Both types of joints have been scoped to single nodes on the surfaces of the bodies to join (see Figure 5). A short section of supports acts as a stiffener (see Figure 5). This section is assigned with a 1000 times stiffer custom steel, it avoids the elements near the nodes scoped for the joints to deform excessively. Bushings are used to formulate a universal joint by defining the stiffness associated with the degrees of freedom to lock between the nodes. A value of $1 \times 10^9\,\mathrm{N\,mm^{-1}}$ is assigned to stiffen the relative translations along x, y, and z (longitudinal axis of the supports) and a value of $1 \times 10^9\,\mathrm{N\,mm/deg}$ assigned to the stiffness of rotations around z.

Results of steady state thermal analysis have been used as imported loads in a static structural study. Pre-load has been applied by defining translation joints and applying joint load as displacement ($\delta = 0.5\,\mathrm{mm}$). Acceleration has been added to simulate the rotation of the assembly in the gravitational field. A negative pressure of 0.1 MPa has been applied to the internal surfaces of the vacuum vessel to simulate the insulation vacuum. A concentrated remote force of components $(5, 2, 0)\mathrm{kN}$ has been applied at position $(-700, 200, -300)\mathrm{mm}$ to simulate an asymmetric response of the system to ensure a more general validation of the model.

Appendix C.2. Results

The internal actions on each support have been probed at the joints for the FEA and calculated by Equation (A1) for the LPM. The results for a series of positions of the gantry are shown in the plot in Figure A3; points show the results of FEAs, dotted lines are sinusoidal functions fitted to the FEAs results, and continuous lines are the results of the LPM. The sinusoidal functions can be described by functions of the form $f(\theta_G) = V_{\mathrm{shift}} + A\sin(\theta_G + \theta_0)$ where V_{shift} is the average value of the function (force, position, or orientation) during a full rotation of the gantry, A is the amplitude, θ_0 the phase, and θ_G the angular position of the gantry.

The plots demonstrate strong agreement between LPM and FEA results. The differences between the two models are reported in Table A1, where they are separated by differences in average force $\Delta_V = V_{\mathrm{shift,LPM}} - V_{\mathrm{shift,FEA}}$ and differences in the force amplitudes $\Delta_A = A_{\mathrm{LPM}} - A_{\mathrm{FEA}}$. The average force differs, in the worst case, by 0.73 kN between LPM and FEA, which is about 0.83% of the average force of 87 kN measured from FEAs. The force amplitudes differ, in the worst case, by 24.6 N or 0.77% in relative terms. These values confirm a good accuracy of the LPM model, with respect to standard simulation methods, to predict forces for an over-constrained architecture.

Table A1. List of absolute and relative errors on the forces for each support, calculated as difference LPM − FEA. Errors are reported as differences between the means and amplitudes of the sinusoidal functions (see Figure A3).

Support	**1**	**2**	**3**	**4**	**5**	**6**	**7**	**8**	
$V_{\mathrm{shift,LPM}}$	87.39	86.36	82.41	84.02	86.36	85.93	82.34	85.61	kN
$V_{\mathrm{shift,FEA}}$	87.83	86.82	82.79	84.39	87.09	86.64	82.71	85.98	kN
Δ_V LPM − FEA	0.45	0.46	0.38	0.37	0.73	0.71	0.37	0.37	kN
Δ_V/FEA	0.51	0.53	0.46	0.44	0.83	0.82	0.45	0.43	%
Amplitude LPM	3.21	3.21	4.88	4.88	5.45	5.45	3.15	3.15	kN
Amplitude FEA	3.18	3.18	4.87	4.87	5.44	5.44	3.14	3.14	kN
Δ_A LPM − FEA	23.35	24.57	14.87	16.63	11.81	12.73	7.38	7.69	N
Δ_A/FEA	0.73	0.77	0.31	0.34	0.22	0.23	0.23	0.24	%

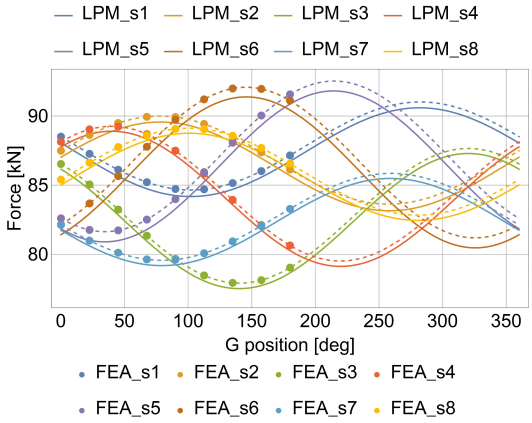

Figure A3. Comparison of the force on each support between the LPM (continuous lines) and FEA (points). Dashed lines fit the FEA data to show agreement where data points have not been simulated.

Table A2. List of absolute and relative errors on the pose calculated as difference LPM − FEA. Errors are reported as differences between the vertical shifts (V-shift) and amplitudes of the sinusoidal functions (see Figure A4).

DOF	e_x	e_y	e_z		θ_x	θ_y	θ_z	
$V_{\text{shift,LPM}}$	0.054	0.010	0.101	mm	0.016	−0.034	−0.029087	mrad
$V_{\text{shift,FEA}}$	0.058	0.010	0.100	mm	0.016	−0.032	−0.029085	mrad
Δ_V LPM − FEA	hl4.065	0.073	0.789	µm	0.036	1.586	0.002143	µrad
Δ_V/FEA	7.045	0.754	0.789	%	0.219	4.904	0.007369	%
Amplitude LPM	0.067	0.132	0.058	mm	0.154	0.011	0.000187	mrad
Amplitude FEA	0.067	0.132	0.058	mm	0.154	0.011	0.000052	mrad
Δ_A LPM − FEA	0.303	0.661	0.318	µm	0.201	0.106	0.135	µrad
Δ_A/FEA	0.452	0.499	0.544	%	0.131	0.928	NR	%

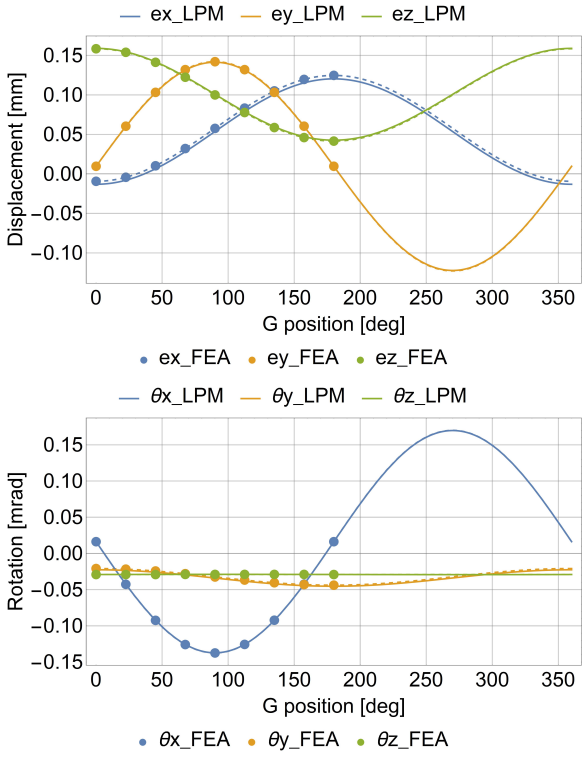

Figure A4. Comparison of the pose (displacement and rotation) of the cold mass between the LPM (continuous lines) and FEA (points). Dashed lines fit the FEA data to show agreement where data points have not been simulated.

For this application especially, estimating the pose of the cold mass is of crucial importance because a supporting system that is not stiff enough can be detrimental to the quality of the cancer treatment to be delivered. Using the methods used in [17], the pose (position and rotation) of the dipole is calculated from FEA results and then compared to the one calculated with the LPM using Equation (A5). As was performed for the internal actions, results of the pose simulations are shown in Figure A4, and quantitative differences between the models are reported in Table A2. The LPM shows a very good qualitative agreement with the FEA.

The differences in average position and rotation between the two models, in the worst case, are about 4 µm and 1.6 µrad. The relative differences for average position and rotation are respectively 7% and 4.9% of the absolute values calculated by FEAs.

Position and rotation amplitude absolute difference between the two models is respectively 0.66 µm and 0.2 µrad. Relative differences are respectively about 0.54% and 0.93%. As can be seen from Figure A4, the absolute amplitude of the rotation around z is almost null. This results in a high relative percentage error when dividing the small absolute difference (0.13 µrad) by an almost null value (0.052 µrad). This high value is non-relevant for the assessment of the accuracy of the LPM.

These values are completely acceptable since the absolute values of 4 µm and 1.5 µrad are much lower than the usual range of accuracy required for these machines (0.3–0.5 mm and 0.3–0.5 mrad at 3σ). The model developed proves its efficacy in studying the application case proposed, a single run of the model reproduces the pose of the cold mass during the rotation of the machine (Figure A4). This gives more complete information about the behavior of forces and displacements during rotation with respect to multiple locally limited FEAs.

References

1. Done, R.; Shaughnessy, B.; Bradshaw, T.; Machin, G.; Evans, B. Cryostat design. In *Cryogenics: Fundamentals, Foundations and Applications*; IOP Publishing: Bristol, UK, 2022.
2. Shu, Q.S.; Demko, J.; Fesmire, J.; Duckworth, R. Design, configuration, and thermal optimization of advanced cryostats. *IOP Conf. Ser. Mater. Sci. Eng.* **2024**, *1301*, 012041. [CrossRef]
3. Piacentini, L.; Dassa, L.; Perini, D.; Ratkus, A.; Torims, T.; Uberti, S. Literature Review of Suspension Systems for cryogenic devices. *Machines* **2023**, *11*, 929. [CrossRef]
4. Liu, Y.; Wang, J.; Wang, L.; Sun, S.; Wang, S.; Yin, L. Design of cold mass supports for a superconducting undulator prototype at SINAP. *IEEE Trans. Appl. Supercond.* **2014**, *25*, 1–4. [CrossRef]
5. Wang, L.; Liu, Y.; Guo, X.; Wang, S.; Li, M.; Sun, S. Development of a Test Cryostat for a Superconducting Undulator Prototype at the SSRF. *IEEE Trans. Appl. Supercond.* **2021**, *31*, 1–5. [CrossRef]
6. Xu, M.F.; Zhang, X.Z.; Ye, R.; Chen, F.S.; Yang, X.C.; Zhao, T.X.; Ge, R. Design, assembly, and pre-commissioning of cryostat for 3W1 superconducting wiggler magnet. *Nucl. Sci. Tech.* **2020**, *31*, 1–15. [CrossRef]
7. Chen, H.H.; Hwang, C.S.; Chang, C.H.; Jan J.C.; Lin, F.Y.; Huang, M.H.; ; Fan, T.C. Design of mechanical structure and cryostat for IASW superconducting wiggler at NSRRC. In Proceedings of the IEEE Particle Accelerator Conference (PAC), Albuquerque, NM, USA, 25–29 June 2007; pp. 374–376.
8. Wang, L.; Wu, H.; Li, S.Y.; Guo, X.L.; Pan, H.; Zheng, S.X.; Green, M.A. Design and analysis of a self-centered cold mass support for the MICE coupling magnet. *IEEE Trans. Appl. Supercond.* **2011**, *21*, 2259–2262. [CrossRef]
9. Meier, J.P.; Bleile, A.; Fischer, E.; Hess, G.; Macavei, J.; Spiller, P. Cryo-technical design aspects of the superconducting SIS100 quadrupole doublet modules. *AIP Conf. Proc.* **2014**, *1573*, 1519–1526.
10. Boulant, N.; Quettier, L. Commissioning of the Iseult CEA 11.7 T whole-body MRI: Current status, gradient–magnet interaction tests and first imaging experience. *Magn. Reson. Mater. Phys. Biol. Med.* **2023**, *36*, 175–189. [CrossRef] [PubMed]
11. Li, L.; Wang, Q.; Zhao, B.; Ni, Z.; Cui, C.; Wang, H. Theoretical model of a cold mass strap suspension system for superconducting magnets. *IEEE Trans. Appl. Supercond.* **2011**, *21*, 3640–3645. [CrossRef]
12. Liu, W.K.; Li, S.; Park, H.S. Eighty years of the finite element method: Birth, evolution, and future. *Arch. Comput. Methods Eng.* **2022**, *29*, 4431–4453. [CrossRef]

13. Liu, W.L.; Xu, Y.D.; Yao, J.T.; Zhao, Y.S. Methods for force analysis of overconstrained parallel mechanisms: A review. *Chin. J. Mech. Eng.* **2017**, *30*, 1460–1472. [CrossRef]
14. Wolfram Research Inc. *Mathematica*; Version 13.0; Wolfram Research Inc.: Champaign, IL, USA, 2021. Available online: https://www.wolfram.com/mathematica (accessed on 1 January 2022).
15. Caprani, C. Virtual Work 3rd Year Structural Engineering. Available online: https://www.colincaprani.com/files/notes/SAIII/Virtual%20Work%201011.pdf (accessed on 12 November 2024).
16. Legnani, G.; Fassi, I.; Giberti, H.; Cinquemani, S.; Tosi, D. A new isotropic and decoupled 6-DoF parallel manipulator. *Mech. Mach. Theory* **2012**, *58*, 64–81. [CrossRef]
17. Piacentini, L.; Dassa, L.; Perini, D.; Ratkus, A.; Torims, T.; Uberti, S. Design of a 6-supports exactly constrained supporting system for superconducting magnets and its application to rotating gantries for cancer therapy. *Meccanica* **2024**, *59*, 2203–2226. [CrossRef]
18. National Institute of Standards and Technologies, Properties of Solid Materials from Cryogenic to Room Temperatures. Available online: https://trc.nist.gov/cryogenics/materials/materialproperties.htm (accessed on 23 October 2024).
19. The HITRIplus Project. Available online: https://www.hitriplus.eu/ (accessed on 23 October 2024).
20. Pullia, M.G.; Felcini, E.; Benedetto, E.; Dassa, L.; De Matteis, E.; Donetti, M.; Frisella, G.; Karppinen, M.; Kurfurst, C.; Mariotto, S.; et al. Gantries for carbon ions. *Health Technol.* **2024**, *14*, 973–983. [CrossRef]

Disclaimer/Publisher's Note: The statements, opinions and data contained in all publications are solely those of the individual author(s) and contributor(s) and not of MDPI and/or the editor(s). MDPI and/or the editor(s) disclaim responsibility for any injury to people or property resulting from any ideas, methods, instructions or products referred to in the content.